Detection of rebars in concrete using advanced ultrasonic pulse compression techniques

[1]S. Laureti, [2]M. Ricci, [3]M.N.I.B. Mohamed, [3]L.A.J. Davis and [3]D.A. Hutchins

[1]Dipartimento di Ingegneria, Università degli Studi di Perugia, 05100 Terni, Italy
[2]Dipartimento di ingegneria Informatica, Modellistica, Elettronica e Sistemistica, Università della Calabria, 87036, Rende (CS), Italy
[3]School of Engineering, University of Warwick, Coventry CV4 7AL, United Kingdom

Abstract

A pulse compression technique has been developed for the non-destructive testing of concrete samples. Scattering of signals from aggregate has historically been a problem in such measurements. Here, it is shown that a combination of piezocomposite transducers, pulse compression and post processing can lead to good images of a reinforcement bar at a cover depth of 55 mm. This has been achieved using a combination of wide bandwidth operation over the 150-450 kHz range, and processing based on measuring the cumulative energy scattered back to the receiver. Results are presented in the form of images of a 20 mm rebar embedded within a sample containing 10 mm aggregate.

1. Introduction

Non-Destructive Testing (NDT) using ultrasound is a well-established method for monitoring concrete structures [1–4]. Ultrasonic NDT (UNDT) has found wide application to concrete in, for example, determining the water-to-concrete ratio [5–8], monitoring of hardening [9,10] and strength [11], detecting damage [12–17] and investigating the condition of reinforcement bars (rebars) [18–21]. Even though the technique has become part of many national standards for concrete diagnostics [22], several of its possible applications are still very challenging and many others are under development. They include the presence of damage, cracks, failures or the integrity of reinforcement bars, when only one side of the structure under-test is available for the inspection.

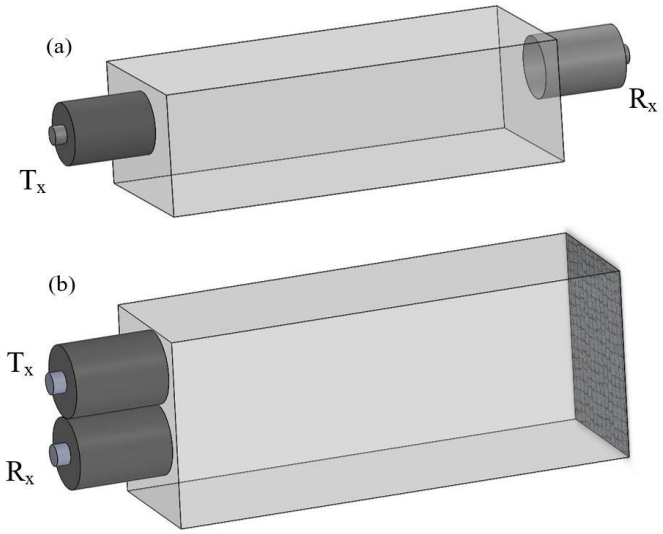

Fig. 1. (a) Through-transmission and (b) pitch-catch transducer inspection arrangement.

The ultrasonic NDT of concrete can be achieved in several different configurations. A single ultrasonic transducer acting as both a transmitter (T_x) and a receiver (R_x) can operate in the pulse-echo configuration. Alternatively, a pair of transducers arranged either in through-transmission or in pitch-catch modes, as depicted in Fig. 1(a) and (b) respectively.

In both cases, the T_x is normally excited by a delta-like pulse voltage signal, which excites the natural resonance frequency of the transducer. The ultrasonic wave packet is then recorded from the R_x after its path into the concrete. The features of interest are retrieved by measuring the time taken by the ultrasonic wave to travel from the T_x to the R_x, *i.e.* Time-of-Flight (ToF) measurements [23,24], or by evaluating the attenuation of the received signal amplitude after its path into the concrete sample [25–27]. In such inspections, cracks, voids but also any functional inclusions such as aggregates or rebars embedded within the concrete act as scatterers for the impinging ultrasonic wave, resulting in a complicated interpretation of echograms. In addition, the presence of aggregates of various dimensions makes concrete highly attenuating towards the acoustic excitation sent, thus limiting the maximum depth of inspection and leading to a poor Signal-to-Noise Ratio (SNR) [28]. It is worth noting that both the attenuation and the scattering magnitude are frequency-dependent, and that they increase if high excitation frequencies are used for concrete ultrasonic inspection [29,30]. For the sake of the SNR enhancement, narrow-bandwidth piezoelectric transducers are usually used, which tend to resonate within a narrow frequency range (typically 50 – 70 kHz and excited with a high-voltage pulse). This is to generate a high energy signal to be delivered into the sample. However, the use of narrow-band transduction

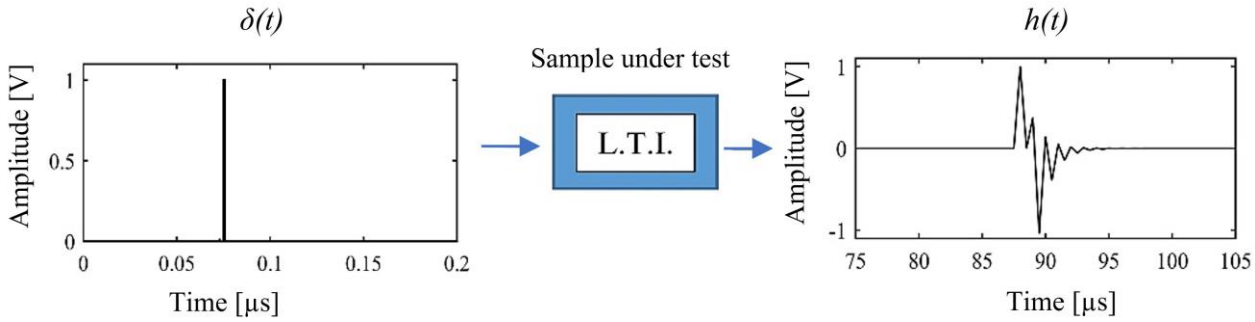

Fig. 2. Impulse response *h(t)* of an LTI system excited by a delta-like *δ(t)* input signal.

systems limits (i) the spatial range resolution, (ii) the lateral resolution and (iii) the features that can be extrapolated from the frequency domain analysis [31,32].

Recently, the use of a coded waveforms such as chirps, together with the Pulse Compression (PuC) technique, has been proven to be a powerful tool for inspecting highly attenuating materials [39,40]. This is because the SNR can be enhanced almost arbitrarily by simply increasing the CodW time duration [41]. The use of coded waveforms and PuC for UNDT in concrete quality assessment has already been reported, either by using transducers in contact with the concrete structure [42,43] or by utilizing air as a coupling medium [32,44]. Furthermore, recent progresses on material research and transducers manufacturing process have led to the fabrication of contact transducers capable of providing longitudinal ultrasonic wave within a broad-band frequency range. PuC thus has the potential to increase the SNR and the imaging capabilities in concrete inspection, especially in term of spatial resolution. However, there is still a need to improve the capability of discriminating between "true" defects and artefacts produced by an erroneous processing of the acquired data. One example is the detection of a true scattering object or defect in the presence of strong back-scatter from aggregate.

In this work, PuC and an original imaging procedure will be used to accomplish the above goal, using (i) a pair of broad-bandwidth piezocomposite transducers to excite the concrete sample under test by longitudinal ultrasonic wave arranged in pitch-catch configuration, and (ii) a low-voltage chirp signal excitation over a frequency range of 150-450 kHz. This combination acts so as to both counterbalance the attenuation and to increase the lateral resolution with respect to standard concrete testing methods. The extended bandwidth is one of the key characteristics that allows pulse compression to be used. It is also worth noting that a pitch-catch configuration was used, as shown in Fig. 1(b). This choice was made to allow extended excitation waveforms, in the form of swept-frequency chirp signals, to be used (these would normally be a problem with pulse-echo measurements, as the drive waveform would mask many received signals from within the sample).

It is also necessary to consider the data analysis which best allows the detection of inclusions, flaws, cracks, voids, reinforcement bars etc within a real concrete sample. Typically, an ultrasonic NDT test would be performed as a B-scan or C-scan, and the peak-to-peak amplitude of the back-propagating signal recorded at each scanned position. Increasingly, imaging procedures capable of improving the spatial resolution by fusing the information from many measurements have been used, such as the Synthetic Aperture Focusing Technique (SAFT) [33,34]. Arrays of ultrasonic transducers can be used in these cases to both speed up the data acquisition and to allow ultrasonic beam shaping via a phased array. As an example, the combination of SAFT and array of ultrasonic transducers at low frequency has been used successfully for imaging back walls, internal layers and reinforcement bars embedded within concrete structures [35–38]. SAFT increases spatial resolution in comparison to standard B-scans or C-scans, and can help to reduce artefacts but it has some drawbacks, the main one being the computational time required. In addition, it does not easily allow an increase in discrimination between defects and backscatter from "natural" inhomogeneities such as aggregate; hence it does not automatically detect the main anomalies present in the structure under such conditions.

Here, an innovative imaging technique is presented capable of identifying the major sources of scattering while significantly reducing the computation time. The technique is based on the extraction and visualization of some features from the cumulative values of the energy reflected back to the receiver. The resultant imaging capability has been tested on the data obtained by scanning across the surface of a concrete sample containing a reinforcement bar (rebar) buried within it. The images obtained have then been compared to standard C-scan images.

2. Theoretical background

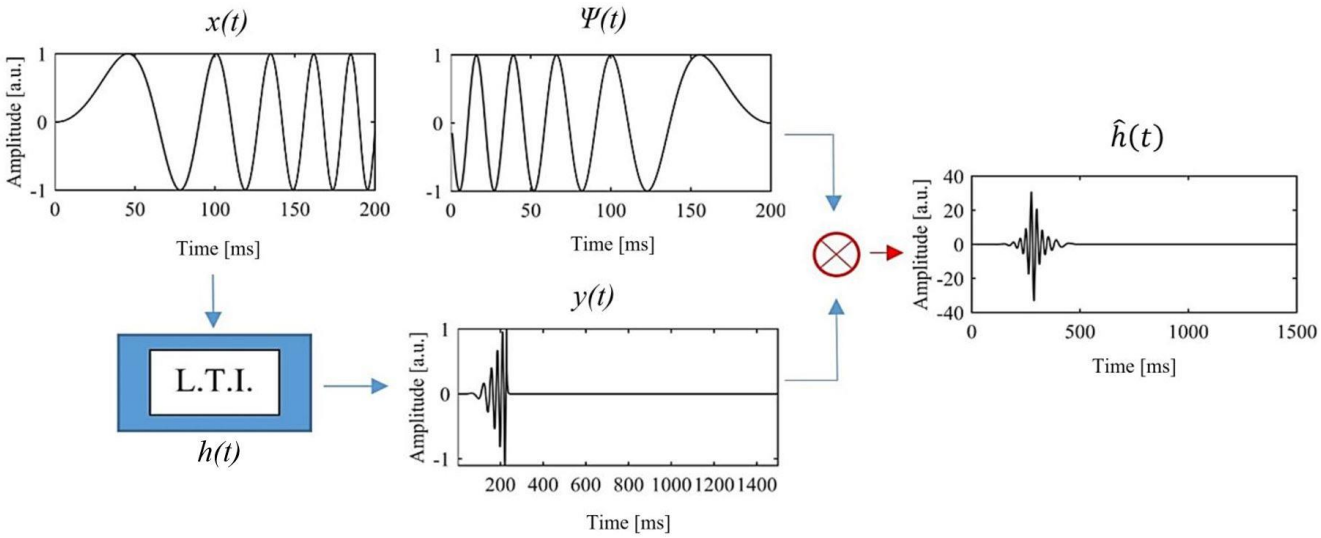

Fig. 3. Pulse compression implementation scheme. *x(t)* is a generic chirp signal used to excite an LTI system, y*(t)* is the recorded output, *Ψ(t)* the matched filter and $\hat{h}(t)$ the estimate impulse response. The red-crossed circle stands for the convolution operator.

The limitations arising by using both delta-like excitations and narrow-band piezoelectric transductions systems can be highlighted by introducing the Linear-Time Invariant (LTI) system and impulse response concepts. This will help the reader to understand the advantages of using a broad-bandwidth transducer and coded signals, here in the form of linear chirp signals, together with the PuC technique.

2.1. LTI systems and Impulse Response

The behaviour of any LTI system is univocally described by its impulse response *h(t)*, which is the time-domain response of such a system when excited by a delta-like input signal *δ(t)*, as shown in Fig. 2. In a real UNDT for concrete inspection, the *δ(t)* voltage driving the T_x is sufficiently low to avoid the onset of non-linear phenomena within the concrete structure under test or in the measurement apparatus, thus allowing the inspected volume to be modelled as an LTI system. Under this hypothesis, the features of interest in any ultrasonic NDT measurement can be extrapolated by analysing the time/frequency behaviour of the measured *h(t)*. Ideally, driving an LTI system by a *δ(t)* input signal corresponds to exciting the system under test across the whole frequency spectrum with a flat constant amplitude. However, the limited bandwidth of any real transduction system acts as band-pass filter for *δ(t)*, thus limiting the frequency range into which the LTI system is effectively excited. Therefore, only an estimate $\hat{h}(t)$ of the *h(t)* can be retrieved, whose quality directly depends on the available frequency bandwidth *B* set by the transduction system used for the test. In particular, the estimate $\hat{h}(t)$ tends to the ideal *h(t)* when $B \to \infty$. Furthermore, the magnitude of the retrieved $\hat{h}(t)$ is related to the physical attenuation given by any medium into which the acoustic energy propagates before being recorded. Therefore, the peak-to-peak amplitude of *δ(t)* should be increased to provide a high SNR. However, driving voltage cannot be enhanced arbitrarily. This is because both safety rules in several industrial environments and physical limits of the transductions systems restrict the maximum applicable driving voltage.

The above constrains can be overcome by the combined use of coded signals for exciting the Tx, here exploited in the form of linear chirp, and the PuC technique for retrieving $\hat{h}(t)$. In effect, the extended time duration of the coded excitation allows more energy to be input into the system than via a short impulse, hence improving performance, but at much lower drive voltages. A general mathematical form of a chirp signal in the continuous time domain *x*(*t*) it is here given:

$$x(t) = \alpha_w(t)\, sin\big(\Phi(t)\big) \qquad (1)$$

which strictly depends from definition of the instantaneous frequency $f_{ist}(t)$, $f_{ist}(t) = \frac{1}{2\pi}\frac{d\Phi(t)}{dt}$, with *Φ(t)* the accumulated signal phase. An example of a chirp signal is depicted in Fig. 3 as *x*(*t*). For a linear chirp signal, the phase is quadratic $\Phi(t) = f_0 t + \frac{B}{2T}t^2$ and the respective instantaneous frequency is linear: $f_{ist}(t) = f_0 + \frac{B}{T}t$. In Eq.(1), $\alpha_w(t)$ is the windowing amplitude modulation of *x(t)* that voids the signal out of the range $t \in [0,T]$, *i.e.* for the chirp duration of interest (*T*). The level of energy being sent towards the sample under test is directly proportional to the time duration *T* of the chirp signal. Moreover, the frequency spectrum can be considered relatively flat around a limited frequency

range. Let $x(t)$ be a generic linear chirp signal sweeping from a lower frequency f_0 to a higher frequency $f_1 = f_0 + B$, with $y(t)$ being the response of an LTI system when excited by $x(t)$. Also, let $\Psi(t)$ be the time-reversed replica of $x(t)$, *i.e.* $\Psi(t) = x(-t)$, as shown in Fig. 3. The estimate $\hat{h}(t)$ of the impulse response $h(t)$ is obtained by performing PuC algorithm, which corresponds in convolving $y(t)$ with $\Psi(t)$:

$$\hat{h}(t) = y(t) \otimes \Psi(t) \tag{2}$$

For the sake of clarity, the PuC algorithm is also depicted schematically in Fig. 4. It can be demonstrated that the SNR gain obtained by using chirp and PuC with respect to the standard pulse-echo technique (with a $\delta(t)$ input signal) applied on a given system with the same overall bandwidth is proportional to the product $T \cdot B$ [41]:

$$SNR\ gain = \frac{SNR_{PuC}}{SNR_{pulse-echo}} = T \cdot B \tag{3}$$

In other words, if the transducer voltage is forced to be kept low and highly attenuating materials have to be inspected, the SNR can be enhanced in any case by increasing T in combination with broad-bandwidth transducers [40].

3. Experimental Setup

3.1. Hardware and Software

The experimental setup used was based on a National Instrument PXI chassis that contained an NI-5412 100 MS/s 14-bit arbitrary waveform generator, and an NI-5105 8 channel 60 MS/s 12-bit digitiser. The ultrasonic transducers were a pair of piezocomposite devices manufactured by EofE Ultrasonics Co. Ltd, Cambridge, UK, having nominal central frequencies f_{ct} = 300 kHz and diameter D_t = 25.4 mm. These are shown in Fig. 4.

Fig. 4. A picture of the employed broad-band piezo-composite transducers.

The experimental activity was performed by arranging the T_x and the R_x in pitch-catch configuration. This choice was made to simulate a concrete structure having a single inspection side available. For the sake of clarity, a sketch of the experimental setup is reported in Fig. 5. For all the

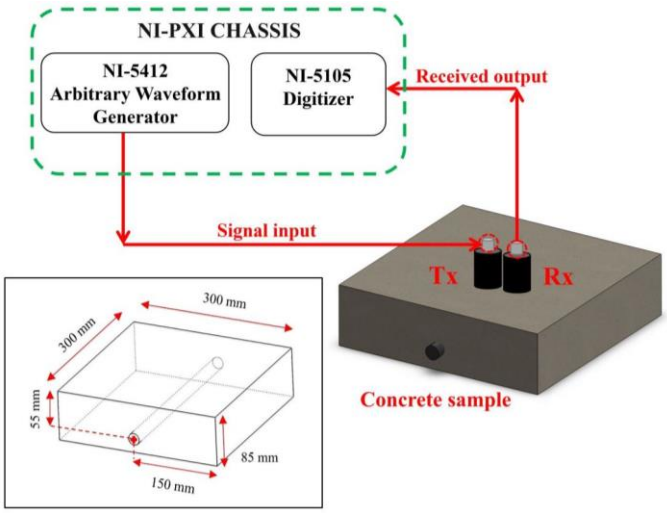

Fig. 5. Sketch of the experimental setup, together with a quoted version of the concrete sample rendering.

reported results, the signal generation/acquisition was managed by a program developed in Labview™ environment, with post-processing achieved using a series of ad hoc Matlab™ scripts.

The chirp signal used for the experimental campaign was a Tukey-windowed linear chirp sweeping from 150 to 450 kHz and having T = 14 ms [45]. Fig. 6(a) and Fig. 6(b) depict the frequency spectrum of the sent and received signal respectively, the last one recorded on a generic sound location:

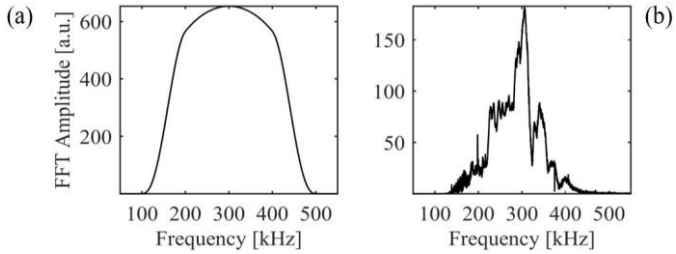

Fig. 6. (a) Input chirp and (b) received signal frequency spectrum.

Note that the peak-to-peak voltage of the input chirp signal used for the experimental measurement was only 12 V, well lower than the normally employed voltage of common commercial ultrasonic NDT instruments.

3.2. Benchmark cast concrete sample

A concrete block with an embedded reinforcement bar was thought to be an appropriate benchmark sample to illustrate the main features of the proposed approach. The concrete sample was cast using Portland cement and a water/10 mm aggregate/sand ratio of 0.5/2.0/2.0. The dimensions of the samples were of 300 by 300 mm, with a thickness of 85 mm. The sample contained steel reinforcement bar at a cover depth of 55 mm. The bar used had a diameter d_{bar} of 20 millimetres (see Fig. 5).

Fig. 7 shows a photograph of the investigated sample, with the transducer pair held rigidly next to each other on

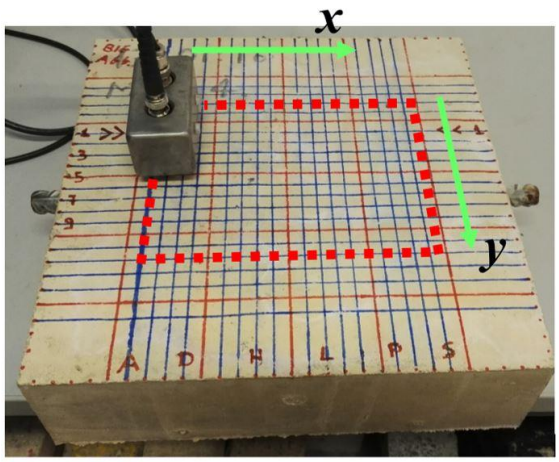

Fig. 7. Concrete with rebar experimental setup sketch.
The red-dotted rectangle shows the limits of the scanning area.

the top surface and oriented parallel to main scanning direction. The scanning area, *i.e.* the red dotted rectangle in Fig. 7, was chosen to be sufficiently far from the edges of the sample, so as to avoid lateral reflections of the ultrasonic beam from the side walls of the concrete sample. The acquisitions followed a grid of points orientated along the x-y axes. In particular, one acquisition was made every 1 centimeter along both the axes, for an overall scanned area of 19 by 14 centimeters.

4. Results

As an example of the type of signals recorded by this system, two estimations of the impulse response $\hat{h}(t)$'s were obtained by exploiting Eq.(2). The line plot in Fig. 8(a) shows the impulse response from scanning locations both above the rebar (red line plot) and well away from the rebar (black line). Fig. 8(b) reports the same graphs plotted in dB. The back-wall echo is clearly visible at about 60 μs (black line plot). In addition, a peak in the cross-correlated signal at approximately 30 μs appear clearly in the red line plot, indicating the presence of the rebar. Since the geometrical center of the bar was located at 55 mm from the scanned surface and the bar radius was 10 mm, the retrieved peak value agrees well with real depth of the bar from the external surface (an estimated value of the sound velocity of 3,200 ms^{-1} was obtained via a through-transmission measurement).

A C-scan arising from the recorded PuC data is shown in Fig. 9. Hence, although the results in Fig. 8 showed promise in the detection of the correct signals, the presence of 10 mm aggregate has obviously affected the image, giving only a blurred outline of the rebar.

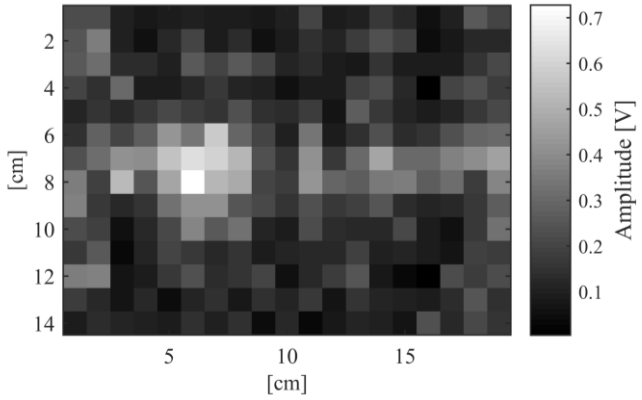

Fig. 9. C-Scan of the concrete with rebar obtained from the $\hat{h}(t)$'s maximum amplitude value at the time range at which the defect echo is expected.

The C-scan relied on detecting the maximum amplitude of the cross-correlated PuC signal envelope within a specific time range (20 – 40 μs in this case, when the expected reflection from the rebar would arrive at the receiver).

It was thought that a clearer image with respect to the standard C-scan could be obtained by carefully extracting several parameters able to show the presence of a rebar. Moreover, such parameters could be chosen so as to avoid any preliminary choice of the time interval of interest, which is a variable that affects the performance of C-

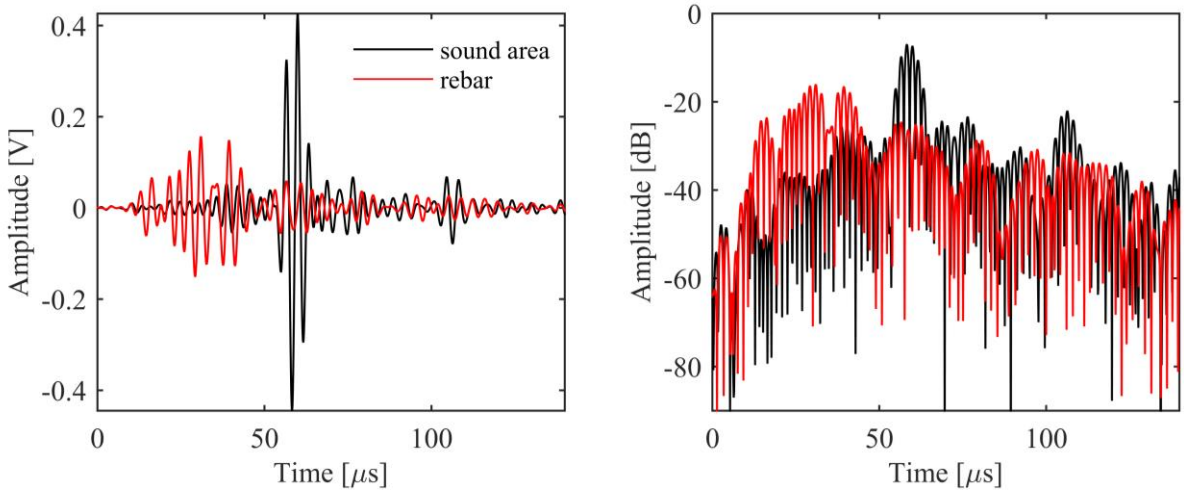

Fig. 8. (a) Received signal after cross-correlation from a sound location compared to the one acquired in a scanning position on the top of the bar. (b) same as (a) but in dB scale.

scans. The idea is that any consistent reflector such as a rebar embedded within the concrete sample should lead to a significant variation in the total reflected energy of the retrieved impulse response, for positions where the transducer pair passed over the rebar. This would expect to be very different to that recorded over regions containing aggregate only, which will still scatter signals back to the receiver, but in a more random way as the transducer pair is scanned over the sample. This effect is best observed by plotting the cumulative (summed) energy at the receiver as a function of time for two fixed locations – one over the rebar, and the other not. This summation is obtained from the responses shown earlier in Fig. 8. The results are shown in Fig. 10. Please note that each cumulative curve has been normalized to their

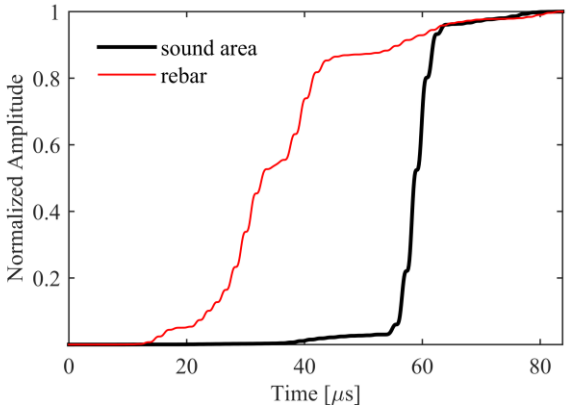

Fig. 10. Normalized cumulative energy at the receiver location for a sound area (black) and for a rebar location (red).

corresponding maximum value.

There are now obvious differences between the two normalized curves. The rebar cumulative energy level increases much more rapidly at earlier times than that scattered back from the aggregate only. This is a clear indication of the presence of a major reflector in that position. Note that the back-wall echo is seen as a steep change in slope at approximately 60 µs.

The data in these curves can be further analyzed to allow images to be produced from the curves obtained from each transducer pair location. A feature extraction algorithm was developed, based on curve-fitting to the cumulative curves retrieved for each scanning point. A Boltzmann function *B(t)* having two free parameters *k* and t_0 was chosen for the fitting, and was of the form

$$B(t) = \frac{1}{1 + e^{-k(t-t_0)}} \qquad (4)$$

The exploited non-linear curve fitting algorithm searched for the optimal values of the parameters *k* and t_0. In this way, a fitted curve was obtained for each retrieved cumulative energy plot. Fig. 11 shows the best-fit curves for the same benchmark locations as in Fig. 10. From these curves, values of the two parameters *k* and t_0 can be plotted as a function of transducer position on the top surface, and an image created. The results are shown in Figs. 12 and 13 respectively as 2D images of the scanned area. The presence of the rebar can now be clearly observed. In both cases there are regions of increased activity away from the rebar, presumably caused by larger or increased concentrations of aggregate. However, it is clear that a big improvement over a standard C-scan obtained from pulse compression data has occurred. Increasingly, the previous features can be fused to

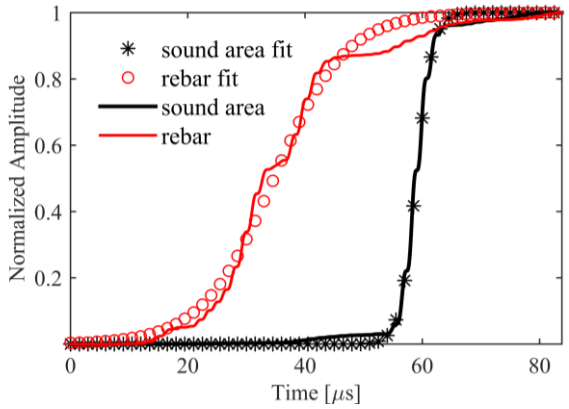

Fig. 11. Normalized cumulative energy for a sound area (black) and its best fit (black star), and for a rebar location (red) and its best fit (red star).

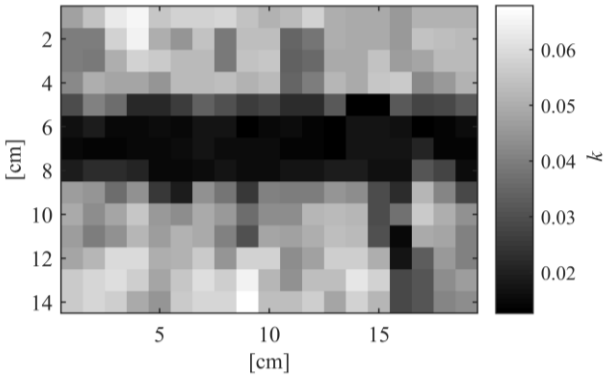

Fig. 12. C-Scan image obtained by plotting the retrieved *k* fit values for each scanned position.

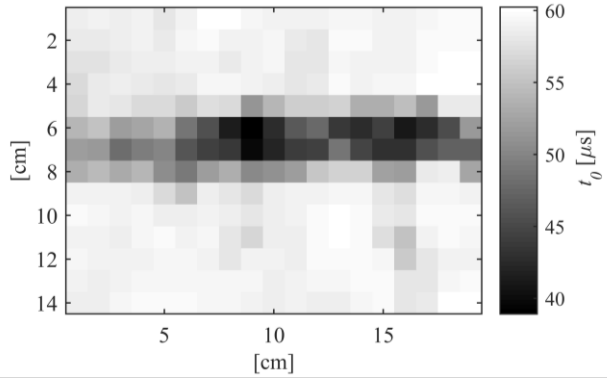

Fig. 13. C-Scan image obtained by plotting the retrieved *k* fit values for each scanned position.

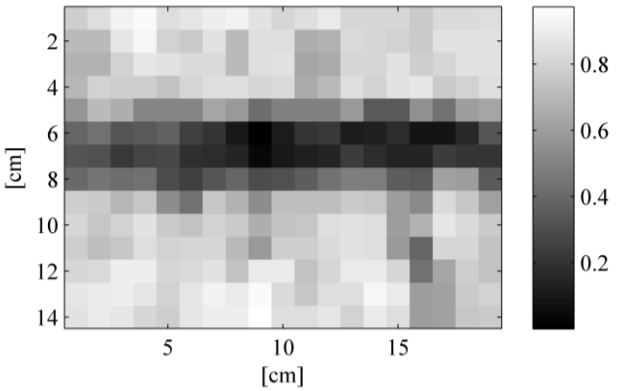

Fig. 14. C-Scan image obtained by plotting the average of k and

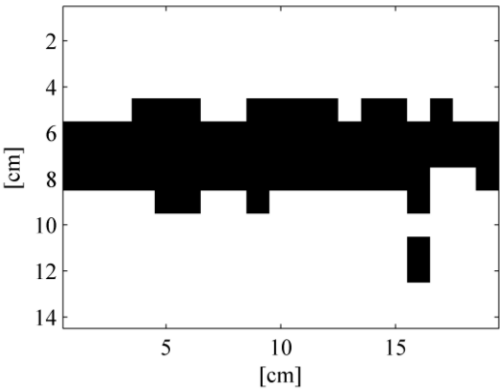

Fig. 15. Binary C-Scan image obtained by applying the Otsu's threshold selection criterion to Fig.14

enhance the image contrast and the resulting images further processed.

For instance, Fig. 14 reports the image achieved by visualizing the average of k and t_0 values after normalization in the range [0,1]. The image of the rebar is even more defined than in the two original images. This can be also seen in Fig. 15, which shows the binary image obtained by applying the Otsu's threshold selection criterion to Fig.14. The shape of the bar is reconstructed quite well and a big aggregate is also recognized in the left-bottom part of the image. Note that binary images obtained with the same automatic procedure from the k and t_0 images (here not reported) are worse.

5. Conclusions

It has been shown that pulse compression is a good tool for the NDT of concrete samples. Using this has allowed signals from rebars to be detected. The combination of wide bandwidth, obtained using piezocomposite transducers, and pulse compression processing via a cross-correlation leads to a measurement of the ultrasonic impulse response. The resulting image can be improved substantially by then applying further data analysis, using the cumulative energy as a measure of the response at each location. This makes the measurement much less susceptible from multiple scattering from aggregate, which is the major problem that limits the NDT of concrete infrastructure.

REFERENCES

[1] J.S. Popovics, J.L. Rose, Survey of developments in ultrasonic NDE of concrete, IEEE Trans. Ultrason. Ferroelectr. Freq. Control. 41 (1994) 140–143.

[2] H.N. Tomsett, The practical use of ultrasonic pulse velocity measurements in the assessment of concrete quality, Mag. Concr. Res. 32 (1980) 7–16.

[3] I.N. Prassianakis, N.I. Prassianakis, Ultrasonic testing of non-metallic materials: Concrete and marble, Theor. Appl. Fract. Mech. 42 (2004) 191–198.

[4] D. McCann, M. Forde, Review of NDT methods in the assessment of concrete and masonry structures, NDT E Int. 34 (2001) 71–84.

[5] E. Ohdaira, N. Masuzawa, Water content and its effect on ultrasound propagation in concrete--the possibility of NDE, Ultrasonics. 38 (2000) 546–52.

[6] Z. Lafhaj, M. Goueygou, A. Djerbi, Correlation between porosity, permeability and ultrasonic parameters of motar with variable water/cement ratio and water content, Cem. Concr. Res. 36.4 (2006) 625-633.

[7] T.P. Philippidis, D.G. Aggelis, An acousto-ultrasonic approach for the determination of water-to-cement ratio in concrete, Cem. Concr. Res. 33 (2003) 525–538.

[8] R. Hooton, S. Popovics, J. Popovics, Ultrasonic Testing to Determine Water-Cement Ratio for Freshly Mixed Concrete, Cem. Concr. Aggregates. 20 (1998) 262.

[9] H. Reinhardt, C. Grosse, A. Herb, Ultrasonic monitoring of setting and hardening of cement mortar—a new device, Mater. Struct. 33 (2000) 581-583.

[10] L.M. Del Río, A. Jiménez, F. López, F.J. Rosa, M.M. Rufo, J.M. Paniagua, Characterization and hardening of concrete with ultrasonic testing, Ultrasonics, 42 (2004) 527–530.

[11] Y. Akkaya, Nondestructive measurement of concrete strength gain by an ultrasonic wave reflection method, Mater. Struct. 36 (2003) 507–514.

[12] J.F. Chaix, V. Garnier, G. Corneloup, Concrete damage evolution analysis by backscattered ultrasonic waves, NDT E Int. 36 (2003) 461–469.

[13] A.A. Shah, Y. Ribakov, S. Hirose, Nondestructive evaluation of damaged concrete using nonlinear ultrasonics, Mater. Des. 30 (2009) 775–782.

[14] S. Ould Naffa, M. Goueygou, B. Piwakowski, F.

Buyle-Bodin, Detection of chemical damage in concrete using ultrasound, Ultrasonics. 40 (2002) 247–251.
[15] A.A. Shah, Y. Ribakov, Non-linear ultrasonic evaluation of damaged concrete based on higher order harmonic generation, Mater. Des. 30 (2009) 4095–4102.
[16] S.F. Selleck, E.N. Landis, M.L. Peterson, S.P. Shah, J.D. Achenbach, Ultrasonic investigation of concrete with distributed damage, ACI Mater. J. 95 (1998) 27–36.
[17] C. Nogueira, K. Willam, Ultrasonic testing of damage in concrete under uniaxial compression, ACI Mater. J. 98 (2001) 265-275.
[18] H.W. Chung, Effects Of Embedded Steel Bars Upon Ultrasonic Testing Of Concrete, Mag. Concr. Res. 30 (1978) 19-25.
[19] B. Ervin, D. Kuchma, Monitoring corrosion of rebar embedded in mortar using high-frequency guided ultrasonic waves, J. Eng. Mech. 1635 (2009) 9–19.
[20] H. Song, V. Saraswathy, Corrosion Monitoring of Reinforced Concrete Structures - A Review, Int. J. Electrochem. Sci. 2 (2007) 1–28.
[21] W.B. Na, T. Kundu, M.R. Ehsani, Ultrasonic guided waves for steel bar concrete interface testing, Mater. Eval. 60 (2002) 437–444.
[22] K. Komloš, S. Popovics, T. Nürnbergerová, B. Babál, J.S. Popovics, Ultrasonic pulse velocity test of concrete properties as specified in various standards, Cem. Concr. Compos. 18 (1996) 357–364..
[23] I. Yaman, G. Inci, N. Yesiller, H.M. Aktan, Ultrasonic pulse velocity in concrete using direct and indirect transmission, ACI Mater. J. 98 (2001) 450–457.
[24] R. Demirboğa, I. Türkmen, M.B. Karakoç, Relationship between ultrasonic velocity and compressive strength for high-volume mineral-admixtured concrete, Cem. Concr. Res. 34 (2004) 2329–2336..
[25] K. Tharmaratnam, B.S. Tan, Attenuation of ultrasonic pulse in cement mortar, Cem. Concr. Res. 20 (1990) 335–345.
[26] W. Suaris, V. Fernando, Ultrasonic Pulse Attenuation as a measure of damage growth during cyclic loading of concrete., ACI Mater. J. 84 (1987) 185–193.
[27] J.W. Ju, L.S. Weng, Y. Liu, Ultrasonic frequency-dependent amplitude attenuation characteristics technique for nondestructive evaluation of concrete, ACI Mater. J. 103 (2006) 177–185.
[28] T.P. Philippidis, D.G. Aggelis, Experimental study of wave dispersion and attenuation in concrete, Ultrasonics. 43 (2005) 584–595.
[29] F. Schubert, B. Koehler, Three-Dimensional Time Domain Modeling of Ultrasonic Wave Propagation in Concrete in Explicit Consideration of Aggregates and Porosity, J. Comput. Acoust. 9 (2001) 1543–1560.
[30] P.A. Gaydecki, F.M. Burdekin, W. Damaj, D.G. John, P.A. Payne, The propagation and attenuation of medium-frequency ultrasonic waves in concrete : a signal analytical approach, Meas. Sci. Technol. 3 (1992) 126–134.
[31] T.H. Gan, D.A. Hutchins, D.R. Billson, D.W. Schindel, The use of broadband acoustic transducers and pulse-compression techniques for air-coupled ultrasonic imaging, Ultrasonics. 39 (2001) 181–194.
[32] P. Purnell, T.H. Gan, D.A. Hutchins, J. Berriman, Noncontact ultrasonic diagnostics in concrete: A preliminary investigation, Cem. Concr. Res. 34 (2004) 1185–1188.
[33] K. Mayer, R. Marklein, K. Langenberg, T. Kreutter, Three-dimensional imaging system based on Fourier transform synthetic aperture focusing technique, Ultrasonics. 28 (1990) 241–255.
[34] R.N. Thomson, Transverse and longitudinal resolution of the synthetic aperture focusing technique, Ultrasonics. 22 (1984) 9–15.
[35] K. Hoegh, L. Khazanovich, Extended synthetic aperture focusing technique for ultrasonic imaging of concrete, NDT E Int. 74 (2015) 33–42.
[36] Z. Hosseini, M. Momayez, F. Hassani, D. Lévesque, Detection of inclined cracks inside concrete structures by ultrasonic saft, AIP Conf. Proc. 975 (2008) 1298–1304.
[37] M. Krause, W. Müller, H. Wiggenhauser, Ultrasonic inspection of tendon ducts in concrete slabs using 3D-SAFT, Acoust. Imaging. (1997) 433-439.
[38] M. Schickert, M. Krause, W. Müller, Ultrasonic Imaging of Concrete Elements Using Reconstruction by Synthetic Aperture Focusing Technique, J. Mater. Civ. Eng. 15 (2003) 235–246.
[39] T.H. Gan, D.A. Hutchins, D.R. Billson, F.C. Wong, Ultrasonic Tomographic Imaging of an Encased, Highly Attenuating Solid Medium, J. Res. 13 (2001) 131–152.
[40] I. Mohamed, D.A. Hutchins, L. Davis, S. Laureti, M. Ricci, Ultrasonic NDE of thick polyurethane flexible riser stiffener material, Nondestructive Testing and Evaluation, (2016) 1-20.
[41] D. Hutchins, P. Burrascano, L. Davis, S. Laureti, M. Ricci, Coded waveforms for optimised air-coupled ultrasonic nondestructive evaluation, Ultrasonics. 54 (2014) 1745–1759.
[42] B. Koehler, G. Hentges, W. Mueller, Improvement of ultrasonic testing of concrete by

combining signal conditioning methods, scanning laser vibrometer and space averaging techniques, NDT E Int. 31 (1998) 281–287.

[43] L. Battaglini, S. Laureti, M. Ricci, P. Burrascano, L.A.J. Davis, D.A. Hutchins, The use of Pulse Compression and Frequency Modulated Continuous Wave to improve Ultrasonic Non Destructive Evaluation of highly-scattering materials, IEEE Int. Ultrason. Symp. IUS, (2014) 1940–1943.

[44] J.R. Berriman, D.A. Hutchins, A. Neild, T.H. Gan, P. Purnell, The application of time-frequency analysis to the air-coupled ultrasonic testing of concrete, IEEE Trans. Ultrason. Ferroelectr. Freq. Control. 53 (2006) 768–776.

[45] P. Pallav, T.H. Gan, D.A. Hutchins, Elliptical-Tukey Chirp Signal for Ultrasonic Imaging, IEEE Trans. Ultrason. Ferroelectr. Freq. Control. 54 (2007) 1530–1540.

[46] N. Otsu, A Threshold Selection Method from Gray-Level Histograms, IEEE Transactions on Systems, Man, and Cybernetics 9, (1979), 62-66.